RESEARCH PAPER

The Study of the Electrochemical and Tribological Behaviors of CrN/AlCrN Coating Deposited by the Arc-PVD Technique

Erfan Lotfi-Khojasteh, Hassan Elmkhah*, Meisam Nouri, Omid Imantalab, Arash Fattah-alhosseini

* *elmkhah@gmail.com & h.elmkhah@basu.ac.ir*

Department of Materials Engineering, Bu-Ali Sina University, Hamedan, 65178-38695, Iran

Received: December 2021 **Revised: November 2022** **Accepted: November 2022**
DOI: 10.22068/IJMSE.2581

Abstract: *This paper aims to study the tribological and electrochemical properties of the CrN/AlCrN nano-layer deposited on H13 tool steel. Arc physical technique was employed to deposit multilayer coating. X-ray diffraction technique, thermionic and field emission scanning electron microscopy and energy dispersive spectroscopy have been used to determine the characteristics of the samples. To study the samples' wear behavior, coating adhesion, and surface hardness, reciprocating wear test, Rockwell-C test, and microhardness Vickers tester were employed, respectively. The measured values of the coefficient of friction and the calculated wear rates showed that the CrN/AlCrN multilayer coating has a much higher wear resistance than the uncoated sample. The coefficient of the friction of the coated sample was 0.53 and that of the uncoated sample was 0.78. Moreover, the wear rate of the coated H13 steel was about 127 times lower than the bare H13 steel sample. The results obtained from electrochemical impedance spectroscopy and polarization tests demonstrated that the corrosion current density of the H13 steel sample was 8 $\mu A/cm^2$ and that of the CrN/AlCrN multilayer-coated sample was 3 $\mu A/cm^2$. In addition, the polarization resistance of the treated and the substrate specimens was estimated at 4.2 and 2.7 $k\Omega.cm^2$, respectively.*

Keywords: *CrN/AlCrN multilayer, Arc-PVD, wear, corrosion, nanostructured.*

1. INTRODUCTION

AISI H13 steel is categorized as high-strength steel and due to its good high-temperature resistance, is commonly used for making casting molds. Elevated hardness and strength and acceptable ductility plus resistance in opposition to wear, erosion, and thermal fatigue are the prominent features of this grade of steel [1, 2]. Physical vapor deposition (PVD) is a superior technique for applying thin films and coatings on industrial alloys that provides a variety of desirable performance properties such as high corrosion resistance, strong resistance against wear, and low friction [3–5]. Arc-PVD is a subset of PVD in which the material evaporation is carried out by an electric arc. This technique has numerous prominent features such as developing a continuous, uniform, and dense coating layer, superior adhesion of the coating to the substrate, controllability of the morphology during the deposition, the ability to deposit materials with high melting temperature, and most importantly, a broad range of coating rates [3, 6–10].

Hard and thin layers of transition metal nitride PVD coatings on tool steels offer an interesting fusion of hardness, wear, and high-temperature chemical stability [11, 12]. Among these coatings, CrN got noticed by the scientific society in the early 1980s due to its good oxidation and friction resistance. The oxidation resistance of CrN coating is caused by the passive surface oxide film formed on the coating. Alloying CrN coatings with aluminum significantly increase their performance [2, 13–17]. The AlCrN system is a semi-stable solid solution that is usually synthesized close to the solubility limit of AlN in CrN. CrN has a cubic crystallographic structure and by increasing the percentage of aluminum in the system, the crystallographic structure will change to hexagonal [18]. For this solid solution with FCC lattice, the hardness value can be increased up to 2900 HV [18, 19]. In addition, AlCrN coatings show high wear resistance against Al_2O_3 abrasives [20, 21]. In recent years, applying AlCrN-based coatings deposited by PVD on industrial tools has dramatically increased the service life in various applications such as cutting, punching, forming, milling, and drilling [22–24].

Using multilayer architecture in a PVD coating stabilizes semi-stable structures and increases the coating's strength, hardness, and corrosion resistance [9, 25–27]. For example, nitride/nitride

[DOI: 10.22068/IJMSE.2581]

multilayer coatings have got attention due to their decent mechanical properties and significant resistance to oxidation and corrosion [29]. The formation of a compact and dense structure in multilayer coatings results in a reduced number of defects, e.g., cracks, holes, and pores, in the coating. This decelerates the penetration of electrolytes into the metallic substrate and makes the multilayer coatings have a higher resistance against corrosion than the single-layer coatings [30]. Researchers have reported that TiN/CrN [8, 30, 31], and ZrN/CrN [7] multilayer coatings have enhanced corrosion and wear behavior compared to single-layer coatings. CrN/AlCrN multilayer coating improves adhesion, wear resistance, and strength compared to AlCrN single-layer coating [13, 32]. The tribological and mechanical properties of the coatings depend on the thickness of the nitrocarburizing layer, surface hardness, surface chemical composition, and microstructure [32–35]. Multilayer coatings are widely used in machining tools and medical applications due to their low coefficient of friction and high wear resistance [17, 32]. Studies have shown that CrN/AlCrN multilayer coatings have decent corrosion resistance which could be due to the ability of Cr to form a passive surface layer. Also, the dense chromium nitride layer does not provide any direct path for the penetration of the corrosive solution [36, 37]. Aluminum improves the structure of the coating and decreases the grain boundaries, which could decelerate the diffusion of the corrosive liquid toward the base alloy. In addition, the presence of aluminum in the coating could result in the formation of a passive aluminum oxide surface film [39].

AISI H13 steel is one of the most widely used materials in the manufacture of die-casting molds. One of the industrial problems of molds is their low resistance to chemical corrosion. With the help of the PVD coating used in this research, it is possible to increase its corrosion resistance. So, the goal of this study was to explore the electrochemical and tribological performance of the CrN/AlCrN multilayer coating deposited by the Arc-PVD technique on AISI H13 steel.

2. EXPERIMENTAL PROCEDURES

The substrate used in this research was H13 tool steel which is compatible with DIN X40CrMoV5-1 (1.2344) and British standard BH13 The samples were rectangular and had 3 × 4 cm dimensions. The surface of the samples was ground with #60 to #800 sandpaper. Then, the samples were placed in a box made of cast iron and filled with cast iron chips. The wall of the cast-iron box was sealed with refractory mud to prevent leakage of air into the box. The cast-iron box was preheated at 600°C in a furnace and then austenitized at 1050°C for one hour in the air and quenched in an oil bath. After cleaning the surface oil, the samples were tempered at 550°C for one hour and cooled down to room temperature in the furnace. After quenching and tempering operations, the samples were ground with sandpapers from number 600 to 2000 to achieve a high-quality surface and remove the scales. Next, the samples were polished with alumina paste for 20 minutes.

The CrN/AlCrN multilayer coating was deposited using a cathodic arc method in a chamber with argon (Ar) and nitrogen (N_2) atmosphere by DS&CA601 Yar-Nikan, Iran. The cathodic arc targets were $Al_{50}Cr_{50}$ for the AlCrN and pure Cr for the CrN layers. After reaching the desired vacuum, the samples were heated. Following the heating, an intermediate layer of Cr/CrN was deposited to improve the bonding between the coating and the substrate, and then, CrN and AlCrN layers were deposited alternately. The coating was applied for 90 min in the -150 V of bias voltage at 200°C substrate temperature, 120 A of cathode arc current, 15 cm of distance between target-to-substrate, and 5×10^{-3} torr of working pressure.

The cross-section of the coating and the alternating layers CrN and AlCrN were evaluated using an FE-SEM. A JEOL JSM-840A scanning electron microscope and a MIRA3 TESCAN–XMU field emission microscope was employed to study the surface and the cross-section of the coating. For X-ray diffraction (XRD) characterization of the phases in the samples, an XMD300 XRD device with a copper radiation source (Cu-K_α) with steps of 0.02 was utilized. To evaluate the quality of the bonding between the coating and the base alloy, a Rockwell C hardness tester was used to apply a normal load of 150 Kgf for 25 seconds. The effect of the indenter was observed by light microscope and compared with VDI 3198 standard [40].

A Microhardness Vickers tester with a load of 25 g was used to measure the hardness of the

[DOI: 10.22068/IJMSE.2581]

samples. To get rid of the effect of the substrate on the measurements, the Jasson-Hogmark approach was applied [41]. A reciprocating ball-on-plate instrument was utilized to examine the frictional behavior of the samples. The settings of the test included a load of 6N and a linear speed of 0.1 m/s for a total sliding distance of 500 m. The balls used in the wear test were Al_2O_3 and the temperature and the humidity during the test were 33°C and 50%, respectively. SEM model JEOL JSM-840A was used to examine the wear tracks and to evaluate the lost volume, and an optical and laser profilometer was used.

Electrochemical analysis was carried out by an Autolab Type III/FRA2 galvanostat/potentiostat instrument. To perform the Tafel polarization test, the samples were inserted in 3.5 wt.% NaCl solution under open circuit potential for 4 hours. Then, potential scanning was performed from -250 to +250 mV relative to the open circuit potential at a rate of 1 mV/s. All tests were accomplished using a standard three-electrode tube, including a silver/silver chloride electrode as the reference electrode, a platinum electrode as the auxiliary electrode, and a test sample as the working electrode in 3.5 wt.% NaCl. Also, the electrochemical impedance spectroscopy (EIS) test was carried out in the frequency range of 100 kHz to 10 mHz and sinusoidal excitation potential of 5 mV.

3. RESULTS AND DISCUSSION

3.1. Composition and Microstructure

The adhesion level of the coating to the substrate was checked out based on the VDI3198 standard [40] and the result is presented in Fig. 1. According to Fig. 1, the quality of the adhesion was excellent and in accordance with the HF1 level of the standard due to the lack of any crack or scaling around the indentation site. The adhesion performance is important since the wear and corrosion properties of the coating strongly depend on the quality of adhesion between the deposited layer and the substrate [42].

As shown in Fig. 2, the peaks observed from the XRD pattern on planes (111), (200), (220), and (311) correspond to CrN and the Cr_2N. The diffraction peaks of the substrate are also seen in the diffraction pattern due to the thin nature of the coating. Due to the high solid solubility of the aluminum element (60- 77% at) in the FCC-CrN phase, no independent diffraction peak was observed for the AlN phase [23, 42, 43]. The dotted lines in Fig. 2 show the expected locations of diffraction peaks for AlN.

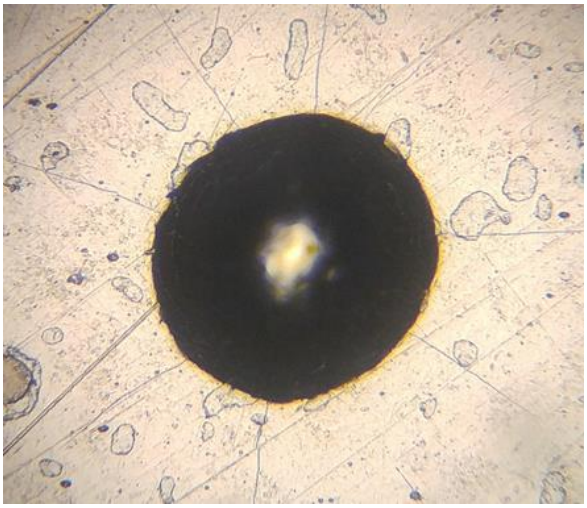

Fig. 1. Optical image of the effect of the Rockwell C indenter to assess adhesion.

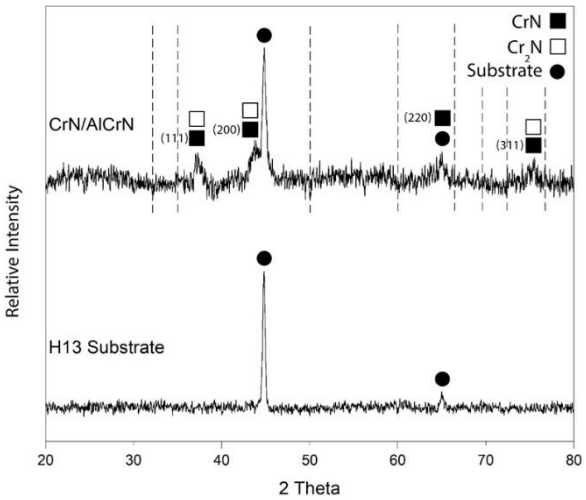

Fig. 2. XRD for CrN/AlCrN coating and H13 substrate samples.

Fig. 3(a) shows an FE-SEM cross-sectional micrograph of the CrN/AlCrN coating. According to the image, the inter-layer Cr/CrN has an approximate thickness of 0.6 µm. The thickness of the bilayers is 62 nm with 14 CrN/CrAlN layers. The bright layers in the micrograph represent the CrN phase and the dark layers represent the AlCrN phase. The thickness of the top layer is equal to 0.3 µm which is made of CrN. Fig. 3(b) shows the EDS line elemental analysis image which was performed from the top coating layer into the substrate alloy. There are some

[DOI: 10.22068/IJMSE.2581]

fluctuations in the concentrations of Cr, Al, and N elements due to the multilayer architecture of the coating. Also, the concentration of Cr is higher than the one of Al. The iron increases gradually toward the substrate which is related to the ferrous-based composition of the substrate.

Fig. 4 shows the FE-SEM and EDS map analysis of the coating surface and macroparticles on the surface. This figure displays the uniform distribution of the elements over the surface, indicating a successful and proper coating process. Moreover, according to the distribution map of aluminum, it can be concluded that there is an accumulation of aluminum elements in the macroparticles on the surface.

3.2. Tribological Behavior of the Coating

The calculated hardness of the H13 substrate and CrN/AlCrN coated sample is 423 ± 9 and 2945 ± 24 HV, respectively. Also, the roughness average (R_a) of the H13 sample and CrN/AlCrN coated sample was measured at 1.1 and 0.06 µm, respectively. The effect of substrate hardness on the measurement was removed using the Jansson-Hogmark approach [40, 44]. According to this method, the hardness of a fine hard coating is calculated according to the equation below:

$$H_F = H_S + \frac{H_C - H_S}{2C\left(\frac{t}{d}\right) + C^2\left(\frac{t}{d}\right)^2} \quad (1)$$

where H_S is the hardness of the substrate, H_F is the hardness of the coating, H_C is the combined hardness of the coating and the substrate obtained through the micro Vickers test, d is the mean diameter of the micro Vickers's indenter effect, t is the thickness of the coating and C is the indenter constant which is considered to be between 0.07 and 0.14 according to the indenter angles [41]. Using Eq. (1), the average coating hardness is reported to be 2945 HV. In AlCrN solid solution the hardness of the single-layer coating can be increased up to 2700- 2900 HV [17, 19].

By creating a multilayer structure with alternating CrN/AlCrN layers, the hardness of the coating can be higher than a single-layer coating.

The COF-distance curves of H13 steel and CrN/AlCrN coating sliding against an Al_2O_3 ceramic ball are shown in Fig. 5. As shown in the figure, the H13 steel sample has a mean coefficient of friction of 0.78, and the CrN/AlCrN coating has a mean COF of 0.53. Therefore, the frictional force is higher for the H13 sample. Fig. 5 demonstrates the three-dimensional profile from the surface of the wear tracks of the H13 steel and the CrN/AlCrN multilayer coating samples. The volume loss was calculated according to Fig. 5 and the wear rate was obtained through Eq. 2 [46]:

$$W = V/(F \times S) \quad (2)$$

Where V is the volume loss (mm^3), F is the applied normal load (N), and S is the sliding distance (m). Based on the results, the wear rate for the substrate H13 alloy is equal to 1.65×10^{-3} mm^3/N.m while the one for the CrN/AlCrN coated sample is as low as 0.013×10^{-3} mm^3/N.m. Thus, the wear rate of the CrN/AlCrN multilayer coating is more than 127 times lower than the one for the H13 substrate sample. In addition, it can be seen that the depth of the wear track in the CrN/AlCrN multilayer sample is 1.4 µm which is less than the thickness of the coating.

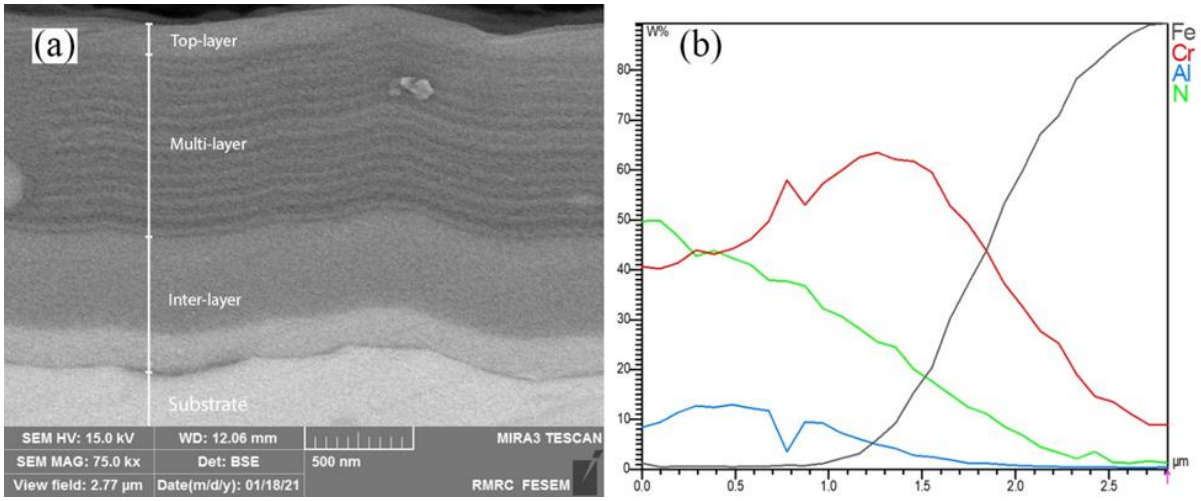

Fig. 3. (a) FE-SEMFE-SEM image and (b) EDS-line of the cross-section of the coated sample.

[DOI: 10.22068/IJMSE.2581]

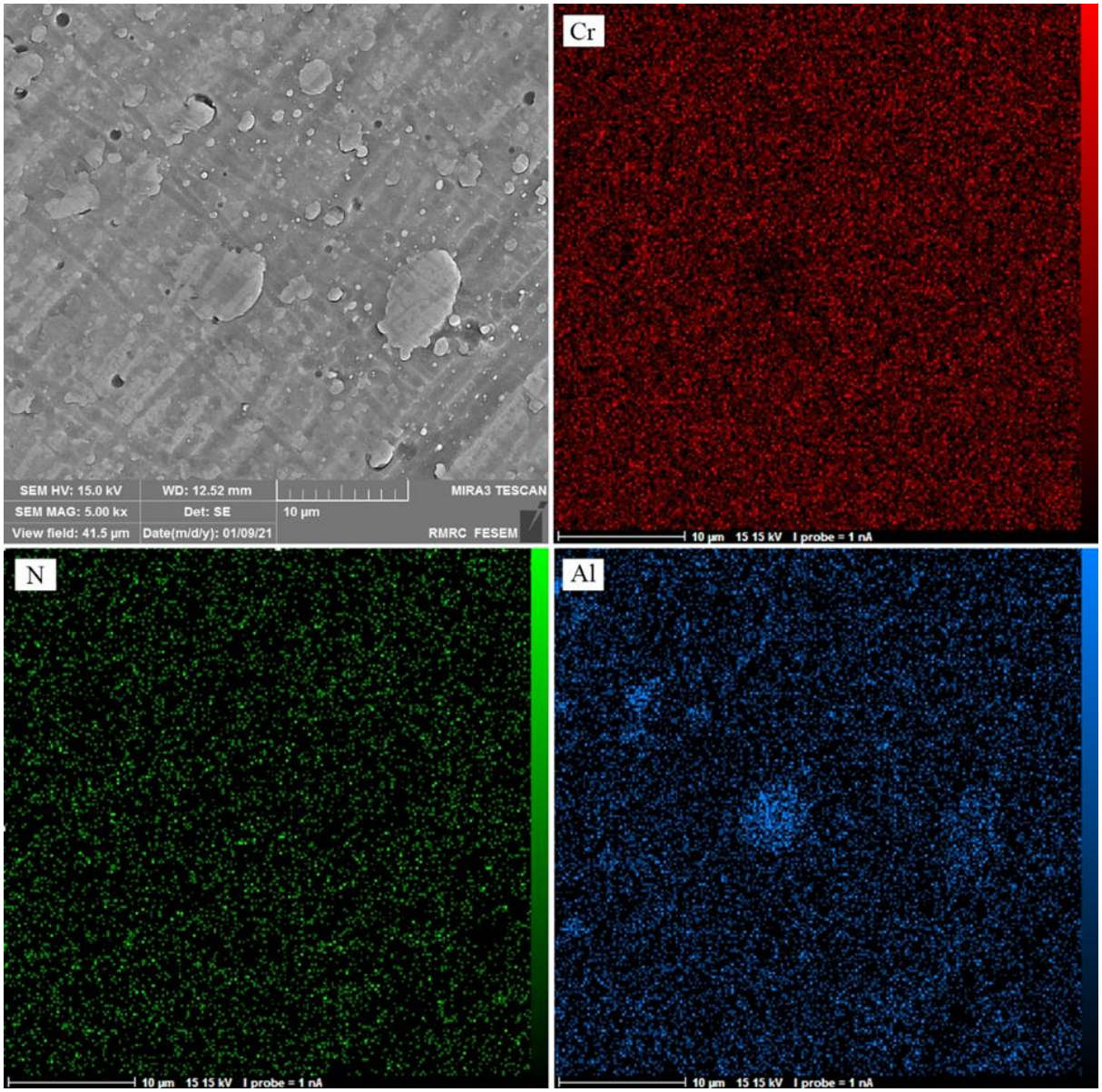

Fig. 4. FE-SEM image and EDS map analysis of CrN/AlCrN multilayer coating surface microparticles on the coating surface.

The wear rate and friction coefficient of the samples are influenced by surface hardness, quality of coating adhesion, applied normal load, and surface roughness of the samples. The deposited CrN/AlCrN coating has a great hardness owing to the hard CrN and AlCrN layers. Moreover, the excellent bonding of the coating to the substrate (Fig. 1) enhances the wear resistance by keeping the coating intact during the sliding motion. The SEM images from the wear tracks are presented in Fig. 6. It can be seen that the width of the worn path of the H13 steel sample is approximately 2000 µm (Fig. 6(a)) while for the CrN/AlCrN multilayer coating, it is approximately 900 µm (Fig. 6(c)). According to Fig. 6(b), the dominant wear mechanism in H13 steel is abrasive wear and a great amount of plastic deformation has occurred on the surface of this sample which can be attributed to the much higher hardness of the Al_2O_3 ceramic ball. In addition, the lower hardness of the H13 steel sample compared to the CrN/AlCrN multilayer coating sample would result in a higher coefficient of friction compared to CrN/AlCrN multilayer coating sample. In the case of the coated sample, the mechanism of wear looks to be

[DOI: 10.22068/IJMSE.2581]

abrasive wear with small regions of fracture on the surface.

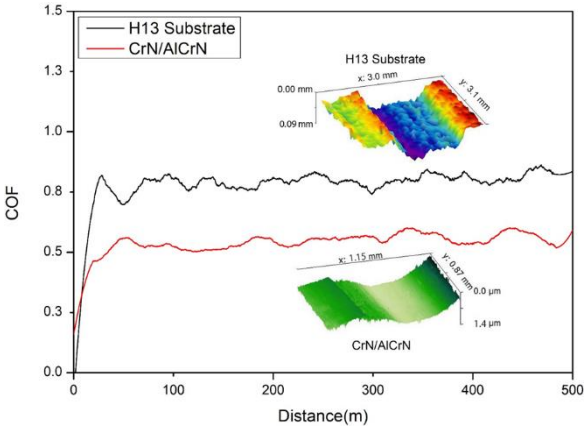

Fig. 5. Coefficient of friction-distance curves of H13 steel and CrN/AlCrN multilayer coating and wear profile of the samples (6 N normal load and 500 m sliding distance).

The wear rate of the CrN/AlCrN multilayer coating is much lower than the H13 steel sample and also the width of the wear track of this coating is thinner (Fig. 6(c)) and the depth of the wear track of the coated sample (Fig. 5) is much shallower than the one of H13 steel sample. All these results confirm the superior wear resistance of the CrN/AlCrN multilayer coating. Fig. 6(d) shows the worn path of the coated sample, this image confirms the excellent wear resistance and low wear rate of this sample. The coating process results in a very hard layer on the surface of the sample that is ~7 times harder than the steel sample.

Fig. 7 shows the wear track of the CrN/AlCrN multilayer coating at higher magnification. According to this image and the results of the EDS analysis, it can be seen that the dominant element at this point is iron, which originated from the substrate and indicates that at this region the CrN/AlCrN coated is peeled off. The high applied normal load (6 N) and the long sliding distance would result in the nucleation and development of cracks at the surface of the coating.

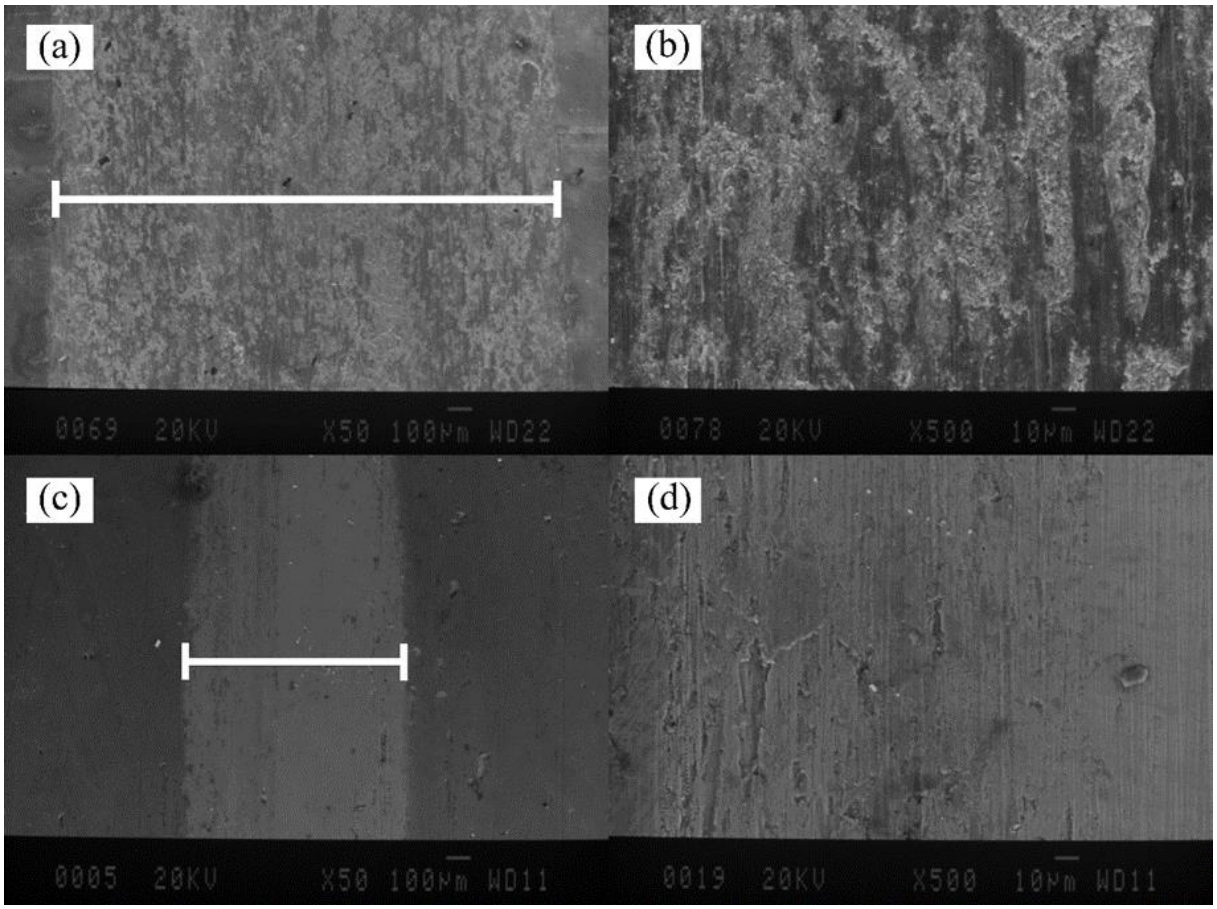

Fig. 6. SEM images of (a) H13 sample wear path ×50, (b) H13 steel wear path ×500, (c) CrN/AlCrN multilayer coating wear path ×50, (d) CrN/AlCrN multilayer coating wear path ×500.

[DOI: 10.22068/IJMSE.2581]

Once the cracks occur, further loading and deformation make cracks extend and propagate. This results in surface fatigue and consequently, brittle fracture of the coating on the surface, producing wear fragments. Other researchers have found that the addition of aluminum to the CrN coating increases the hardness, increases Young's modulus, decreases the grain size, increases the anti-scaling property, and increases the oxidation resistance of the sample [14, 21]. It should also be noted that the CrN coating exhibits better anti-friction properties than the AlCrN coating [14].

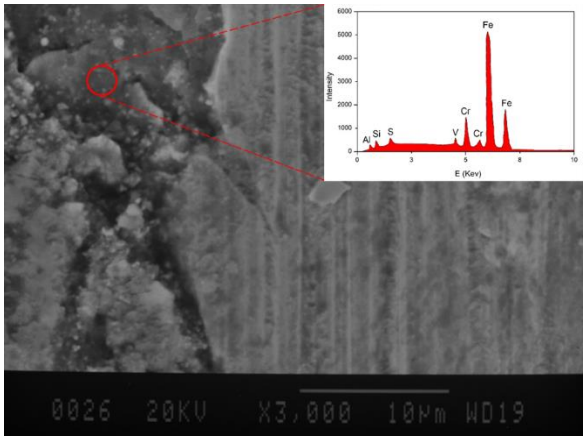

Fig. 7. SEM image and EDS elemental analysis of the CrN/AlCrN multilayer coating wear path

3.3. Corrosion Behavior

Fig. 8 shows the Tafel polarization curves for the H13 steel substrate and the CrN/AlCrN multilayer coating sample after 4 hours of immersion in 3.5 wt.% NaCl solution under the open circuit potential. According to Fig. 8, it is clear that the corrosion current density of the coated sample is smaller than the one of the substrate alloy. The linear parts in both the cathodic and anodic branches close to the corrosion potential describe the Tafel anodic and cathodic behavior [47, 48]. In addition, the corrosion potential of the coated sample (-530 mV) is nobler than the corrosion potential of the H13 substrate (-560 mV). The corrosion current densities of the H13 steel substrate and the CrN/AlCrN multilayer coating were calculated as about 8 and 3 µA/cm^2, respectively, using the slope of the areas shown in Fig. 8(a).

The smaller corrosion current density of the CrN/AlCrN multilayer coating manifests higher corrosion resistance in this sample [49]. A major problem with coatings created by the PVD process is the formation of defects such as pores and pinholes, which provide suitable paths for the diffusion of the solution toward the substrate and affect the corrosion behavior of the coating. Therefore, reducing or eliminating the defects of the coating increases polarization resistance.

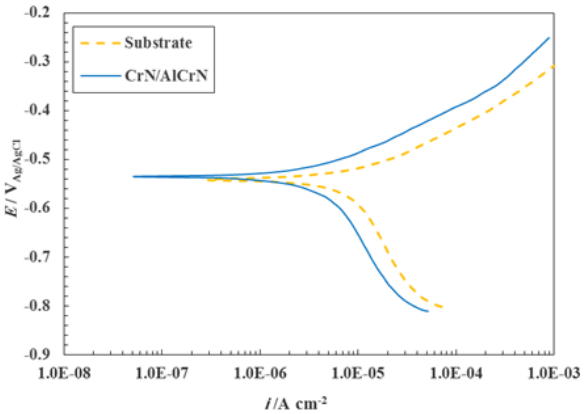

Fig. 8. Tafel polarization curve for the H13 steel sample and the CrN/AlCrN multilayer coating in 3.5 wt.% NaCl solution.

Table 1 summarizes the values of the electrochemical parameters extracted from the Tafel polarization curves.

Fig. 9(a) shows the Nyquist plot of the samples studied in this research in the form of Nyquist curves. According to this figure, non-ideal capacitive behavior is observed for both samples. The diameter of the capacitive loops in the Nyquist curves is attributed to the polarization resistance. Therefore, according to Fig. 8, the coated sample has a higher polarization resistance compared to the substrate. This result is consistent with those of the Tafel test. In addition, according to Fig. 9(a), the polarization resistance of the CrN/AlCrN multilayer coating and H13 steel substrate samples can be estimated as about 4.2 and 2.7 kΩ.cm^2, respectively. According to the bode plots (Fig. 9(b)), three points can be expressed.

Table 1. Electrochemical parameters derived from the Tafel polarization curves of studied samples

Sample	E_{corr} (mV)	i_{corr} (µA cm^{-2})	β_a (mV/ dec)	β_c (mV/ dec)
Substrate	-560	8.01	80	320
CrN/AlCrN	-530	3.12	87	340

[DOI: 10.22068/IJMSE.2581]

First, the total impedance of the CrN/AlCrN coated sample is higher than that of the substrate. The second, it is seen capacitive response of the spectra in middle to low-frequency range and a resistive response in the high-frequency range. Finally, the capacitive behavior is not pure. The simulated electrical equivalent circuit (EEC) and the values of electrical elements obtained by Nova 1. 11 software can present further detailed data about the experimental EIS spectra.

Two different EECs indicated in Fig. 10 were considered to fit the experimental EIS results of the substrate and multilayered coating system [50, 51]. The EEC for the substrate is indicated in Fig. 10(a).

It includes a solution resistance (R_s) between the tip of the Luggin capillary and the working electrode, a charge transfer resistance (R_1) related to the solution/substrate interface, and a double-layer capacitance (CPE_1). This is common to use this EEC (Fig. 10(a)) for the simple corrosion system and it is well-known that the constant phase element (CPE) relating to surface inhomogeneities is inserted in EECs instead of the capacitance for a better quality fitting. Generally, An EEC with two CPEs is used to simulate the experimental EIS results of the coating systems to justify the electrochemical behavior at sub-interfaces (electrolyte/substrate and coating electrolyte). As indicated in Fig. 10(b), R_s denotes the solution resistance, R_2, and CPE_2 associated with the coating resistance, and the capacitance of the coating, originating from the presence of the micro-defects could act as preferred corrosion sites at the coating/electrolyte interface, R_1 and CPE_1 is about the charge transfer resistance and double-layer capacitance ascribed to occurrence of electrochemical reactions at substrate/electrolyte interface [52]. As can be seen in Fig. 9, the impedance data fitting with the EECs (Fig. 10) show a good fit for the experimental EIS data over the whole frequency range.

Table 2 summarizes the values of electrical parameters obtained from the fitting of EIS data.

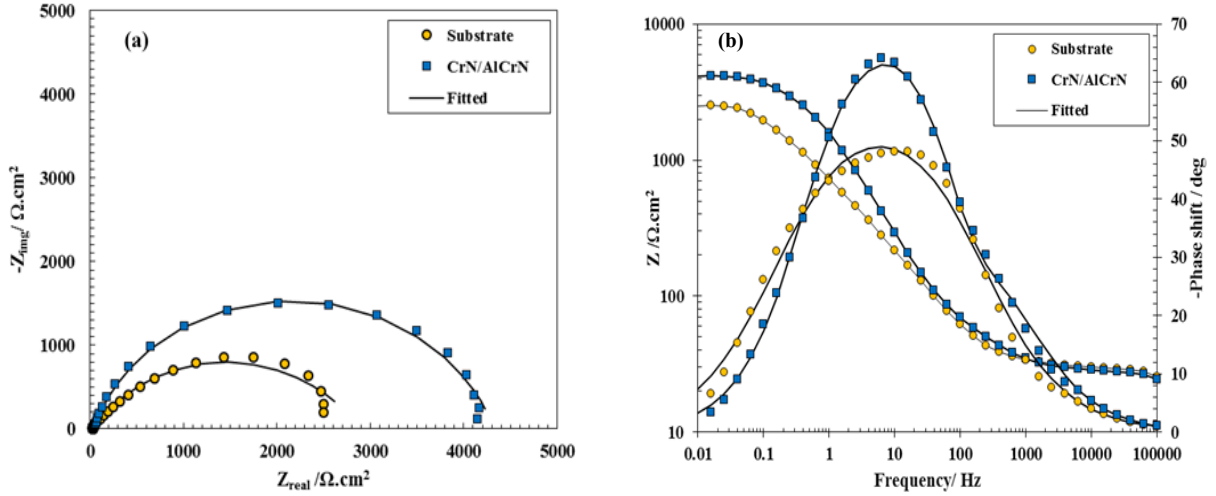

Fig. 9. (a) Nyquist and (b) bode plots of the H13 steel sample and the CrN/AlCrN multilayer coating in 3.5 wt.% NaCl solution. Symbols and solid lines are experimental EIS data and fitting results, respectively.

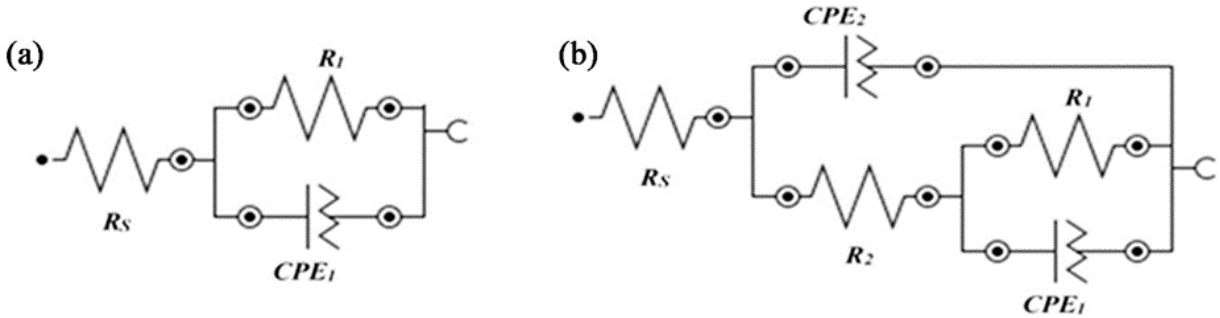

Fig. 10. The electrical equivalent circuit employed in the fitting procedure of the experimental EIS: (a) substrate and (b) CrN/AlCrN multilayer coating.

[DOI: 10.22068/IJMSE.2581]

Table 2. Electrochemical parameters derived from the experimental EIS data for the studied samples in a 3.5 wt% NaCl solution

Sample	R_s ($\Omega.cm^2$)	R_1 ($\times10^3\ \Omega.cm^2$)	Q_1 ($\times10^{-6}\ S^{\alpha}.\Omega^{-1}.cm^{-2}$)	n_1	R_2 ($\times10^3\ \Omega.cm^2$)	Q_2 ($\times10^{-6}\ S^{\alpha}.\Omega^{-1}.cm^{-2}$)	n_2	R_p ($\times10^3\ \Omega.cm^2$)
Substrate	27.21	2.883	323.07	0.64	-	-	-	2.883
CrN/AlCrN	25.90	3.857	16.00	0.88	0.351	124.57	0.76	4.208

samples in a 3.5 wt% NaCl solution

The polarization resistance (R_p) of the coating system could be determined by the sum of R_{ct} and R_c. Accordingly, it can be expressed from Table 2 that the CrN/AlCrN multilayer coating represented higher polarization resistance than that of the substrate. It can be qualitatively noted that CrN/AlCrN multilayer coating with dense microstructure and few permeable defects could resist the penetration of the corrosive media to the substrate.

It can be concluded that the CrN/AlCrN multilayer coating sample possesses higher corrosion resistance. The higher corrosion resistance of the coated sample is ascribed to the presence of alternating and dense layers of CrN and AlCrN. The presence of aluminum and chromium in the multilayer coating provides the coating with higher passivation against corrosion and better electrochemical behavior that prevents the diffusion of the electrolyte solution toward the substrate [49]. In addition, the presence of aluminum in the CrN structure makes the structure denser and also leads to a decrease in grain boundaries which will improve the corrosion resistance of the coating [39].

4. CONCLUSION

1. Multilayer coating of CrN and AlCrN by alternating layers increases the hardness of CrN/AlCrN coating compared to single-layer CrN and AlCrN coatings.
2. Deposition of CrN/AlCrN multilayer coating on the H13 steel substrate reduces the coefficient of friction and wear rate. The H13 steel sample has a mean friction coefficient of 0.78 and the CrN/AlCrN coated sample has an average friction coefficient of 0.53. Also, the wear rate of the H13 sample is 1.65×10^{-3} $mm^3/N.m$ and the wear rate of the CrN/AlCrN coated sample is 0.013×10^{-3} $mm^3/N.m$.
3. The measured values of COF and wear rate show superior wear resistance of the CrN/AlCrN multilayer treated sample. The higher wear resistance of the coating can be ascribed to the great hardness, low roughness, chemical composition, and multilayer coating architecture of the deposited layer.
4. The results of polarization and EIS tests show that the corrosion current density of the H13 steel sample and CrN/AlCrN multilayer coating are 8 and 3 $\mu A/cm^2$, respectively. Also, the polarization resistance of the coated and substrate samples can be estimated at 4.2 and 2.7 $k\Omega.cm^2$, respectively.
5. The smaller corrosion current density and larger polarization resistance of the multilayer-coated sample can be associated with the multilayer architecture, the density of the coating, the presence of aluminum and chromium elements, and the formation of a passive layer on the coating surface.

REFERENCES

[1] S. H. Chang, Y. K. Lin, K. T. Huang, Study on the thermal erosion, wear and corrosion behaviors of TiAlN/oxynitriding duplex-treated AISI H13 alloy steel, Surf. Coatings Technol. 207 (2012) 571–578.

[2] Y. Birol, Sliding wear of CrN, AlCrN and AlTiN coated AISI H13 hot work tool steels in aluminium extrusion, Tribol. Int. 57 (2013) 101–106.

[3] A Mubarak, E. Hamzah, M. R. M. Toff, Review of physical vapour deposition (PVD) techniques for hard coating, J. Mek. 20 (2005) 42–51.

[4] T. Savisalo, D. B. Lewis, Q. Luo, M. Bolton, P. Hovsepian, Structure of duplex CrN/NbN coatings and their performance against corrosion and wear, Surf. Coatings Technol. 202 (2008) 1661–1667.

[5] G. Cappelletti, L. D'Avico, R. Beltramin, E. Pargoletti, S. P. M. Trasatti, Insight into the Release Agents/PVD Coatings Interaction for Plastic Mold Technology, Coatings, 10 (2020) 281.

[6] M. D. Huang, Y. Liu, F. Y. Meng, L. N. Tong, P. Li, Thick CrN/TiN multilayers

[DOI: 10.22068/IJMSE.2581]

deposited by arc ion plating, Vacuum. 89 (2013) 101–104.

[7] P. Mohamadian Samim, A. Fattah-Alhosseini, H. Elmkhah, O. Imantalab, Structure and corrosion behavior of ZrN/CrN nano-multilayer coating deposited on AISI 304 stainless steel by CAE-PVD technique, J. Asian Ceram. Soc. 8 (2020) 460–469.

[8] E. Lotfi-Khojasteh, M. Sahebazamani, H. Elmkhah, M. Nouri, O. Imantalab, A. Fattah-Alhosseini, A study of the electrochemical and tribological properties of TiN/CrN nano-layer coating deposited on carburized-H13 hot-work steel by Arc-PVD technique, J. Asian Ceram. Soc. 9 (2021) 270-282.

[9] L. D'Avico, R. Beltrami, N. Lecis, S.P. Trasatti, Corrosion behavior and surface properties of PVD coatings for mold technology applications, Coatings. 9 (2019) 1–12.

[10] S. Y. Yoon, J. K. Kim, K. H. Kim, A comparative study on tribological behavior of TiN and TiAlN coatings prepared by arc ion plating technique, Surf. Coatings Technol. 161 (2002) 237–242.

[11] H. C. Barshilia, K. S. Rajam, Structure and properties of reactive DC magnetron sputtered TiN/NbN hard superlattices, Surf. Coatings Technol. 183 (2004) 174–183.

[12] A. I. Kalinichenko, E. Reshetnyak, V. Strel'nitskij, G. Abadias, Role of nonlocal thermoelastic peaks in the stress and texture evolution of TiN coatings formed by plasma based ion implantation and deposition, Surf. Coatings Technol. 391 (2020) 125695.

[13] K. Jokar, H. Elmkhah, A. Fattah-alhosseini, K. Babaei, A. Zolriasatein, Comparison of the wear and corrosion behavior between CrN and AlCrN coatings deposited by Arc-PVD method, Mater. Res. Express. 6 (2019) 116426.

[14] J. L. Mo, M.H. Zhu, Sliding tribological behaviors of PVD CrN and AlCrN coatings against Si_3N_4 ceramic and pure titanium, Wear. 267 (2009) 874–881.

[15] J. L. Endrino, G. S. Fox-Rabinovich, C. Gey, Hard AlTiN, AlCrN PVD coatings for machining of austenitic stainless steel, Surf. Coatings Technol. 200 (2006) 6840–6845.

[16] T. Sampath Kumar, A. Vinoth Jebaraj, Metallurgical characterization of CrN and AlCrN physical vapour deposition coatings on aluminium alloy AA 6061, Mater. Today Proc. 22 (2019) 1479–1488.

[17] Y. Vengesa, A. Fattah-alhosseini, H. Elmkhah, O. Imantalab, Surface & Coatings Technology Influence of post-deposition annealing temperature on morphological, mechanical and electrochemical properties of CrN/CrAlN multilayer coating deposited by cathodic arc evaporation- physical vapor deposition process, Surf. Coat. Technol. 432 (2022) 128090.

[18] M. Kawate, A. Kimura, T. Suzuki, Microhardness and lattice parameter of $Cr_{1-x}Al_xN$ films, J. Vac. Sci. Technol. A Vacuum, Surfaces, Film. 20 (2002) 569–571.

[19] A. E. Reiter, B. Brunner, M. Ante, J. Rechberger, Investigation of several PVD coatings for blind hole tapping in austenitic stainless steel, Surf. Coatings Technol. 200 (2006) 5532–5541.

[20] R. Franz, Abrasive and Adhesive Wear Behavior of Arc-Evaporated $Al_{1-x}Cr_xN$ Hard Coatings, (2010) 605–611.

[21] X. Z. Ding, X. T. Zeng, Structural, mechanical and tribological properties of CrAlN coatings deposited by reactive unbalanced magnetron sputtering, Surf. Coatings Technol. 200 (2005) 1372–1376.

[22] K. Bobzin, E. Lugscheider, R. Nickel, N. Bagcivan, A. Krämer, Wear behavior of $Cr_{1-x}Al_xN$ PVD-coatings in dry running conditions, Wear. 263 (2007) 1274–1280.

[23] W. Kalss, A. Reiter, V. Derflinger, C. Gey, J. L. Endrino, Modern coatings in high performance cutting applications, Int. J. Refract. Met. Hard Mater. 24 (2006) 399–404.

[24] A. E. Reiter, V.H. Derflinger, B. Hanselmann, T. Bachmann, B. Sartory, Investigation of the properties of $Al_{1-x}Cr_xN$ coatings prepared by cathodic arc evaporation, Surf. Coatings Technol. 200 (2005) 2114–2122.

[25] E. Spain, J. C. Avelar-Batista, M. Letch, J. Housden, B. Lerga, Characterisation and

[DOI: 10.22068/IJMSE.2581]

applications of Cr-Al-N coatings, Surf. Coatings Technol. 200 (2005) 1507–1513.
[26] R. Raab, C. M. Koller, S. Kolozsvári, J. Ramm, P. H. Mayrhofer, Interfaces in arc evaporated Al-Cr-N/Al-Cr-O multilayers and their impact on hardness, Surf. Coatings Technol. 324 (2017) 236–242.
[27] S. PalDey, S. C. Deevi, Single layer and multilayer wear resistant coatings of (Ti, Al)N: A review, Mater. Sci. Eng. A. 342 (2003) 58–79.
[28] M. Fenker, M. Balzer, H. Kappl, Corrosion protection with hard coatings on steel: Past approaches and current research efforts, Surf. Coatings Technol. 257 (2014) 182–205.
[29] M. Nordin, M. Larsson, S. Hogmark, Mechanical and tribological properties of multilayered PVD TiN/CrN, TiN/MoN, TiN/NbN and TiN/TaN coatings on cemented carbide, Surf. Coatings Technol. 106 (1998) 234–241.
[30] Y. L. Chipatecua, J. J. Olaya, D. F. Arias, Corrosion behaviour of CrN/Cr multilayers on stainless steel deposited by unbalanced magnetron sputtering, Vacuum. 86 (2012) 1393–1401.
[31] Z. A. Fazel, H. Elmkhah, A. Fattah-Alhosseini, K. Babaei, M. Meghdari, Comparing electrochemical behavior of applied CrN/TiN nanoscale multilayer and TiN single-layer coatings deposited by CAE-PVD method, J. Asian Ceram. Soc. 8 (2020) 510–518.
[32] N. S. Mansoor, A. Fattah-alhosseini, H. Elmkhah, A. Shishehian, Electrochemical behavior of TiN, CrN and TiN/CrN nanostructured coatings on the nickel-chromium alloy used in dental fixed prosthesis, J. Asian Ceram. Soc. 8 (2020) 694–710.
[33] S. Kumar, S. R. Maity, L. Patnaik, Friction and tribological behavior of bare nitrided, TiAlN and AlCrN coated MDC-K hot work tool steel, Ceram. Int. 46 (2020) 17280–17294.
[34] A. Bahrami, S. H. M. Anijdan, M. A. Golozar, M. Shamanian, N. Varahram, Effects of conventional heat treatment on wear resistance of AISI H13 tool steel, Wear. 258 (2005) 846–851.
[35] M. Ueda, K. Uchino, T. Senuma, Effects of carbon content on wear property in pearlitic steels, Mater. Sci. Forum. 426–432 (2003) 1175–1180.
[36] H. Goto, Y. Amamoto, Effect of varying load on wear resistance of carbon steel under unlubricated conditions, Wear. 254 (2003) 1256–1266.
[37] C. Gaona-Tiburcio, M. Montoya-Rangel, J. A. Cabral-Miramontes, F. Estupiñan-López, P. Zambrano-Robledo, R. O. Cruz, J. G. Chacón-Nava, M. Á. Baltazar-Zamora, F. Almeraya-Calderón, Corrosion resistance of multilayer coatings deposited by PVD on Inconel 718 using electrochemical impedance spectroscopy technique, Coatings. 10 (2020) 1–11.
[38] I. E. Hossein Olia, Reza Ebrahimi-Kahrizsangi, Fakhreddin Ashrafizadeh, The corrosion study of TiN, TiAlN, and CrN multilayer coatings deposit on martensitic stainless steel by arc cathodic physical vapor deposition, Mater. Res. Express. 6 (2019) 046425.
[39] B. Zhang, J. Wang, Y. Zhang, G. Han, F. Yan, Comparison of tribocorrosion behavior between 304 austenitic and 410 martensitic stainless steels in artificial seawater, RSC Adv. 6 (2016) 107933–107941.
[40] N. Vidakis, A. Antoniadis, N. Bilalis, The VDI 3198 indentation test evaluation of a reliable qualitative control for layered compounds, J. Mater. Process. Technol. 143–144 (2003) 481–485.
[41] B. Jönsson, S. Hogmark, Hardness measurements of thin films, Thin Solid Films. 114 (1984) 257–269.
[42] B. Lenz, H. Hasselbruch, A. Mehner, Automated evaluation of Rockwell adhesion tests for PVD coatings using convolutional neural networks, Surf. Coatings Technol. 385 (2020) 125365.
[43] Y. Makino, Prediction of phase change in pseudobinary transition metal aluminum nitrides by band parameters method, Surf. Coatings Technol. 193 (2005) 185–191.
[44] A. Sugishima, H. Kajioka, Y. Makino, Phase transition of pseudobinary Cr-Al-N films deposited by magnetron sputtering method, Surf. Coatings Technol. 97 (1997) 590–594.
[45] L. A. Dobrzański, M. Polok, M. Adamiak,

[DOI: 10.22068/IJMSE.2581]

Structure and properties of wear resistance PVD coatings deposited onto X37CrMoV5-1 type hot work steel, J. Mater. Process. Technol. 164–165 (2005) 843–849.

[46] K. Singh, P.K. Limaye, N. L. Soni, A. K. Grover, R. G. Agrawal, A. K. Suri, Wear studies of (Ti-Al)N coatings deposited by reactive magnetron sputtering, Wear. 258 (2005) 1813–1824.

[47] S. Vafaeian, A. Fattah-alhosseini, M. K. Keshavarz, Y. Mazaheri, The influence of cyclic voltammetry passivation on the electrochemical behavior of fine and coarse-grained AISI 430 ferritic stainless steel in an alkaline solution, J. Alloys Compd. 677 (2016) 42–51.

[48] A. Ebrahimi, H. Esfahani, O. Imantalab, A. Fattah-Alhosseini, Biological, antibacterial activities and electrochemical behavior of borided commercially pure titanium in BSA-containing PBS, Trans. Nonferrous Met. Soc. China. 30 (2020) 944–957.

[49] V. Prabakaran, C. Kavitha, Characterisation and Corrosion Resistance of TiCrN Composite Coating on Steel by Physical Vapour Deposition Method, J. Bio- Tribo-Corrosion. 2 (2016) 1–6.

[50] A. Ebrahimi, H. Esfahani, A. Fattah-alhosseini, O. Imantalab, In-vitro electrochemical study of TiB/TiB_2 composite coating on titanium in Ringer's solution, J. Alloys Compd. 765 (2018) 826–834.

[51] M. Molaei, A. Fattah-Alhosseini, S. O. Gashti, Sodium Aluminate Concentration Effects on Microstructure and Corrosion Behavior of the Plasma Electrolytic Oxidation Coatings on Pure Titanium, Metall. Mater. Trans. A Phys. Metall. Mater. Sci. 49 (2018) 368–375.

[52] B. Feizi Mohazzab, B. Jaleh, O. Kakuee, A. Fattah-alhosseini, Formation of titanium carbide on the titanium surface using laser ablation in n-heptane and investigating its corrosion resistance, Appl. Surf. Sci. 478 (2019) 623–635.

[DOI: 10.22068/IJMSE.2581]